The Astrophysical Journal Letters, 752:L12 (6pp), 2012 June 10 doi:10.1088/2041-8205/752/1/L12

UBIQUITOUS TORSIONAL MOTIONS IN TYPE II SPICULES

B. De Pontieu[1], M. Carlsson[2], L. H. M. Rouppe van der Voort[2], R. J. Rutten[2], V. H. Hansteen[1,2], and H. Watanabe[3]
[1] Lockheed Martin Solar & Astrophysics Laboratory, Org. A021S, Building 252, 3251 Hanover Street, Palo Alto, CA 94304, USA; bdp@lmsal.com
[2] Institute of Theoretical Astrophysics, University of Oslo, P.O. Box 1029, Blindern, N-0315 Oslo, Norway
[3] Unit of Synergetic Studies for Space, Kyoto University, 17 Kitakazan Ohmine-cho, Yamashina, Kyoto 607-8471, Japan
Received 2012 April 10; accepted 2012 May 9; published 2012 May 24

ABSTRACT

Spicules are long, thin, highly dynamic features that jut out ubiquitously from the solar limb. They dominate the interface between the chromosphere and corona and may provide significant mass and energy to the corona. We use high-quality observations with the Swedish 1 m Solar Telescope to establish that so-called type II spicules are characterized by the simultaneous action of three different types of motion: (1) field-aligned flows of order 50–100 km s^{-1}, (2) swaying motions of order 15–20 km s^{-1}, and (3) torsional motions of order 25–30 km s^{-1}. The first two modes have been studied in detail before, but not the torsional motions. Our analysis of many near-limb and off-limb spectra and narrowband images using multiple spectral lines yields strong evidence that most, if not all, type II spicules undergo large torsional modulation and that these motions, like spicule swaying, represent Alfvénic waves propagating outward at several hundred km s^{-1}. The combined action of the different motions explains the similar morphology of spicule bushes in the outer red and blue wings of chromospheric lines, and needs to be taken into account when interpreting Doppler motions to derive estimates for field-aligned flows in spicules and determining the Alfvénic wave energy in the solar atmosphere. Our results also suggest that large torsional motion is an ingredient in the production of type II spicules and that spicules play an important role in the transport of helicity through the solar atmosphere.

Key words: Sun: chromosphere – Sun: corona – Sun: magnetic topology – Sun: oscillations

Online-only material: color figure

1. INTRODUCTION

Between the photosphere and corona lies the chromosphere, a region of relatively cool plasma that is most conspicuous in the hydrogen Hα Balmer line. The upper chromosphere is dominated by spicules, thin jets of chromospheric plasma that reach heights of 10,000 km or more above the photosphere. Although spicules were described already by Secchi in 1877, understanding their physical nature has progressed only slowly (reviews by Beckers 1968; Sterling 2000). The launch of the *Hinode* satellite (Kosugi et al. 2007) and the combined use of adaptive optics and image post-processing (van Noort et al. 2005) in ground-based observing have revolutionized our view of spicules.

There are (at least) two types (De Pontieu et al. 2007b). Type I spicules reach heights of 2–9 Mm, show upward and downward velocities of 10–30 km s^{-1}, and have lifetimes of 3–10 minutes. They probably correspond to on-disk dynamic fibrils caused by shock waves that propagate upward into the chromosphere (Hansteen et al. 2006; Rouppe van der Voort et al. 2007; De Pontieu et al. 2007a; see also Suematsu et al. 1995). Type II spicules reach larger heights at velocities of order 50–100 km s^{-1}. They have shorter lifetimes, of order 100 s, and usually only exhibit upward motion before their rapid fading in the chromospheric lines in which they are detected. On the disk they appear as rapidly moving absorption features in the blue wings of chromospheric lines (Langangen et al. 2008; Rouppe van der Voort et al. 2009). In this Letter, we focus on this intriguing class of features.

Our previous studies suggest that type II spicules represent impulsively accelerated chromospheric material that is continuously heated while it rises (De Pontieu et al. 2009, 2011). The cause of the heating and acceleration is unknown, but a magnetic process such as reconnection and/or flux emergence is most likely (De Pontieu et al. 2007b; Sterling et al. 2010; Martínez-Sykora et al. 2011).

Type II spicules show other motions in addition to radial outflow. In the Ca II H line they are seen to sway to-and-fro transversely with amplitudes of order 10–20 km s^{-1} and periodicities of 100–500 s, suggesting Alfvénic waves (De Pontieu et al. 2007c). The continuation of these motions in transition region and coronal lines suggests that they may help drive the solar wind (McIntosh et al. 2011).

Other types of motion are less well established. Suematsu et al. (2008) reported that some spicules appear as double threads with evidence of spinning motion. Curdt & Tian (2011) and Curdt et al. (2012) suggest that similar spinning explains the tilts of ultraviolet lines in the so-called explosive events producing larger-scale macro spicules. Spectral-line tilts were noted earlier in observations at the limb and also attributed to spicule rotation (Beckers 1972), or not interpreted (Houtgast & Namba 1979).

In this Letter, we definitely confirm the indications for twisting spicular motions by unequivocally detecting torsional spicule modulation in limb spectroscopy and imaging spectroscopy with unprecedented spectral and spatial resolution.

2. OBSERVATIONS

We analyze various data sets obtained with the Swedish 1 m Solar Telescope (SST; Scharmer et al. 2003) on La Palma: slit spectroscopy with the TRI-Port Polarimetric Echelle-Littrow (TRIPPEL) spectrograph (Kiselman et al. 2011) and imaging spectroscopy with the CRisp Imaging SpectroPolarimeter (CRISP; Scharmer et al. 2008). All observations used adaptive optics.

With the TRIPPEL spectrograph we observed the Ca II H line at 396.8 nm with nominal spectral resolution of 1.6 pm.

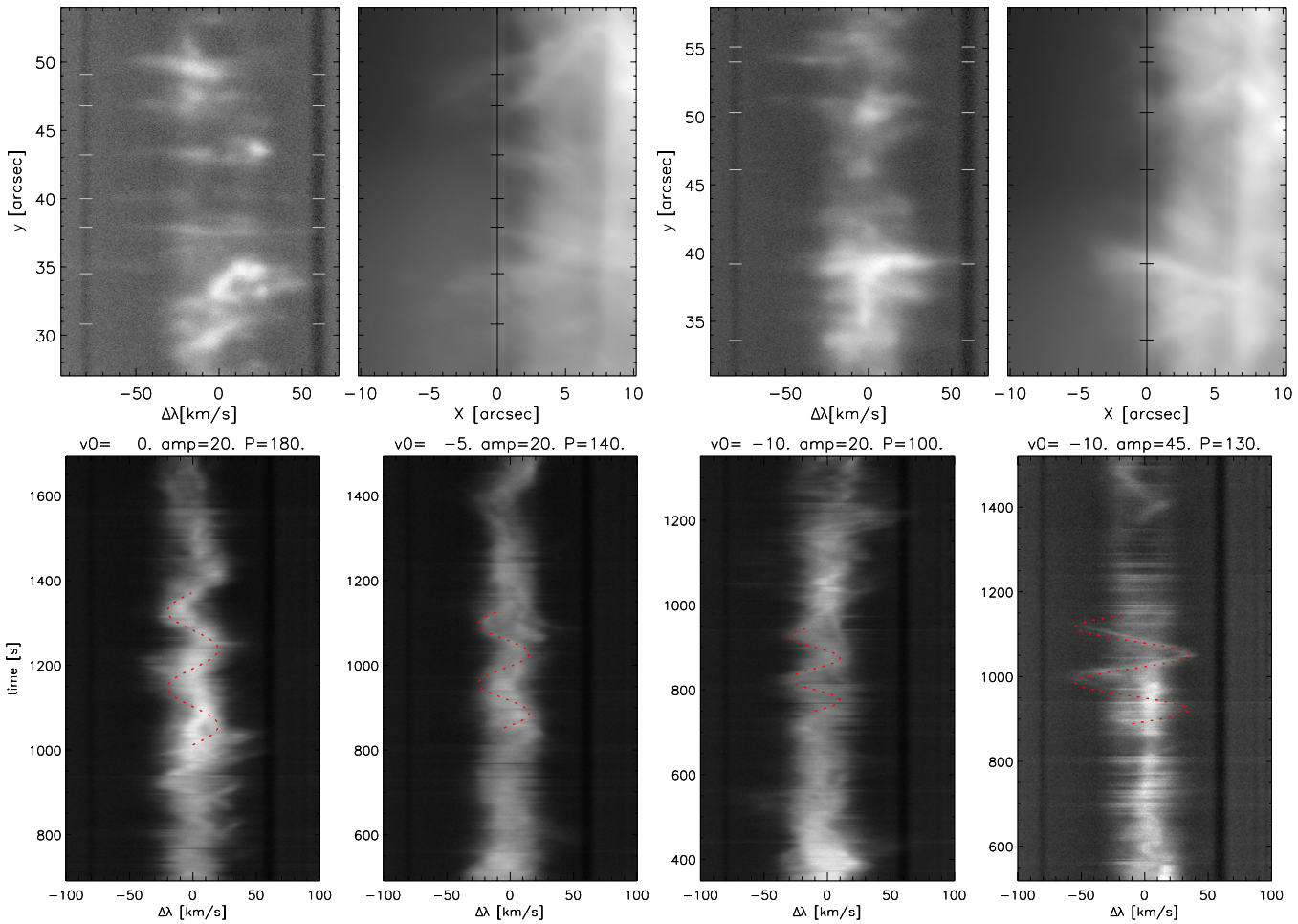

Figure 1. Examples of large torsional motion in off-limb spicules in Ca II H. Top row shows the spatial variation of the Ca II H profile, with the right-hand panel of each pair a slit-jaw image with the off-limb intensities enhanced with a radial filter. These show spicules protruding upward from the limb, which is to the right. The left-hand panels are the corresponding Ca II H spectrograms. The black line in the slit-jaw images shows the slit location. The spectrograms are dominated by linear features that are often tilted from the horizontal dispersion direction, a clear signature of torsional motions, typically over 20–40 km s^{-1}. Selected spicules are marked by black ticks in the slit-jaw images and white ticks in the spectrograms. Bottom row shows examples of large swaying motion in off-limb spicules in Ca II H. Each panel shows the temporal evolution of the Ca II H profile. Despite significant superposition of multiple oscillatory signals there are often episodes of quasi-sinusoidal oscillation. For guidance we have overplotted sinus curves with the amplitude ("amp" in km s^{-1}) and period (P in s) specified in each legend.

(A color version of this figure is available in the online journal.)

A slit-jaw camera of the same type was slaved to the spectrum camera. The data were binned to 0.49 pm spectral and 0.″068 spatial pixel sizes. The spectrograms were corrected for dark current, gain variations, and spectrograph distortions following Langangen et al. (2007). We use a 55 minute duration, 0.91 s cadence sequence of Ca II H spectrograms taken on 2009 October 8 in excellent seeing. The slit was set parallel to the limb at various heights above the limb ranging from 3″ to 10″. The exposure time was 800 ms.

CRISP contains a dual Fabry–Pérot interferometer and allows for fast (<50 ms) wavelength tuning within a spectral region. High spatial resolution and precise alignment between the sequentially taken images for different tunings are achieved with the image restoration technique of van Noort et al. (2005) and Rouppe van der Voort et al. (2009). In Section 3, we present results from two CRISP data sets: a 17 minute sequence at the ultra-high cadence of 0.44 s sampling Hα (656.3 nm) only at $\pm$1204 mÅ ($\pm$55 km s^{-1}), registering the limb near AR11230 on 2011 June 11, and an earlier 36 minute, 17 s cadence sequence of finely spaced Hα and Ca II 854.2 nm profile samplings registering the limb on 2010 June 27.

3. RESULTS

Our various observations all show clear evidence of torsional motions on very small scales, of order 0.″7 or less. We first demonstrate these in the TRIPPEL spectra. Since the slit was oriented approximately parallel to the limb, it crossed many spicules. In Figure 1 (top row) we show two λ–y cuts, selecting moments when the slit was located at least several arcseconds above the limb to avoid the enormous line-of-sight superposition at and just above the limb. The slit-jaw images indeed show many distinct spicules that seem at least partially resolved. Each spectral λ–y panel contains multiple cases in which a spicule appears as a thin bright streak across the spectrum, with a small tilt from the horizontal wavelength direction and a substantial offset from nominal line center. We detected such behavior throughout the 55 minute sequence at all sampled heights. The tilted-streak morphology indicates relative redshift on one side of a spicule, blueshift on the other. This reversal in transverse motion is the signature of torsional spicule motion. In addition, the substantial offsets of the tilted streaks from the nominal line center can be understood as the superposition of swaying

motion and a projection of field-aligned flow onto the line of sight.

Next, we examine how our data can be used to separate and constrain the magnitudes and other properties of these three types of spicular motion. Figure 1 (bottom row) shows the temporal variation of the Ca II H profile. Although significant line-of-sight superposition occurs, we find clear evidence of quasi-sinusoidal episodes in the Doppler shifts. To get an idea of the typical amplitudes and periods of such oscillations we overplot simple functions $v = v_0 + a\sin(2\pi(t-t_0)/P)$ and find that amplitudes of order 20–40 km s^{-1} and periods of order 100–200 s are common. Swaying and torsional motions can both produce such sinusoidal signature in $\lambda-t$ plots, but they have a different appearance in a time sequence of successive $\lambda-y$ plots, with swaying motions showing wiggling of the entire streak-like feature whereas torsional modulation shows up as a tilted streak that shrinks into a more vertical feature and then becomes tilted with opposite sign. Detailed inspection of many such plots showed that temporal undulation as in Figure 1 (bottom row) is sometimes associated with swaying and sometimes with torsional modulation.

Our data inspection thus reveals evidence for three distinct types of spicular motion. Given the limitations of our data sets (in particular the enormous line-of-sight superposition at the limb and variations in seeing quality), we find that the best method to derive statistical properties of these different motions is to compare the observations with Monte Carlo simulations. We adopt the methodology used previously by De Pontieu et al. (2007c) and McIntosh et al. (2008): we consider N spicules and impose on each a field-aligned flow v_p, a torsional motion v_t, and a swaying motion v_s. Inspired by our earlier analyses of type II spicules we assume that, during their lifetime T, they continuously grow with constant velocity v_p along a straight path, inclined by an angle α from the vertical and with an azimuth angle β, until they fade rapidly from view. The torsional and swaying motions are assumed to have periods P_t and P_s, respectively, with random phase.

Figures 2 and 3 show examples of comparisons between observed λ–y and $\lambda-t$ plots and results from these Monte Carlo simulations for different parameter choices. We made many such plots with large parameter variation and defined a best-fit solution by selecting parameter combinations that reproduce the observed behavior the best. Per spicule this best-fit choice takes v_p randomly from a Gaussian distribution around 60 km s^{-1} with standard deviation $\sigma = 10$ km s^{-1} (similar to what is found by T. M. D. Pereira et al. 2012, in preparation), T from a Gaussian distribution around 120 s with $\sigma = 30$ s (T. M. D. Pereira et al. 2012, in preparation), α from a Gaussian distribution around 20° with $\sigma = 10°$ (based on slit-jaw images), β from a uniform distribution over 0°–360°, v_t from a Gaussian distribution around 30 km s^{-1} with $\sigma = 10$ km s^{-1}, v_s from a Gaussian distribution around 15 km s^{-1} with $\sigma = 5$ km s^{-1}, and both P_s and P_t from a uniform distribution over 100–300 s. Comparison of the $\lambda-y$ and $\lambda-t$ panels for this best-fit solution with the observations in the top left panels of Figures 2 and 3 and in Figure 1 shows that the best-fit solution reproduces, statistically, the appearance of both types of data, with a similar multitude of slightly tilted streak-like features in λ–y and similar sinusoidal swings in $\lambda-t$.

How well defined are the best-fit parameters, given the large number of free parameters in our simulations? To answer this question we ran multiple simulations in which we changed the distribution for only one parameter, keeping all others fixed.

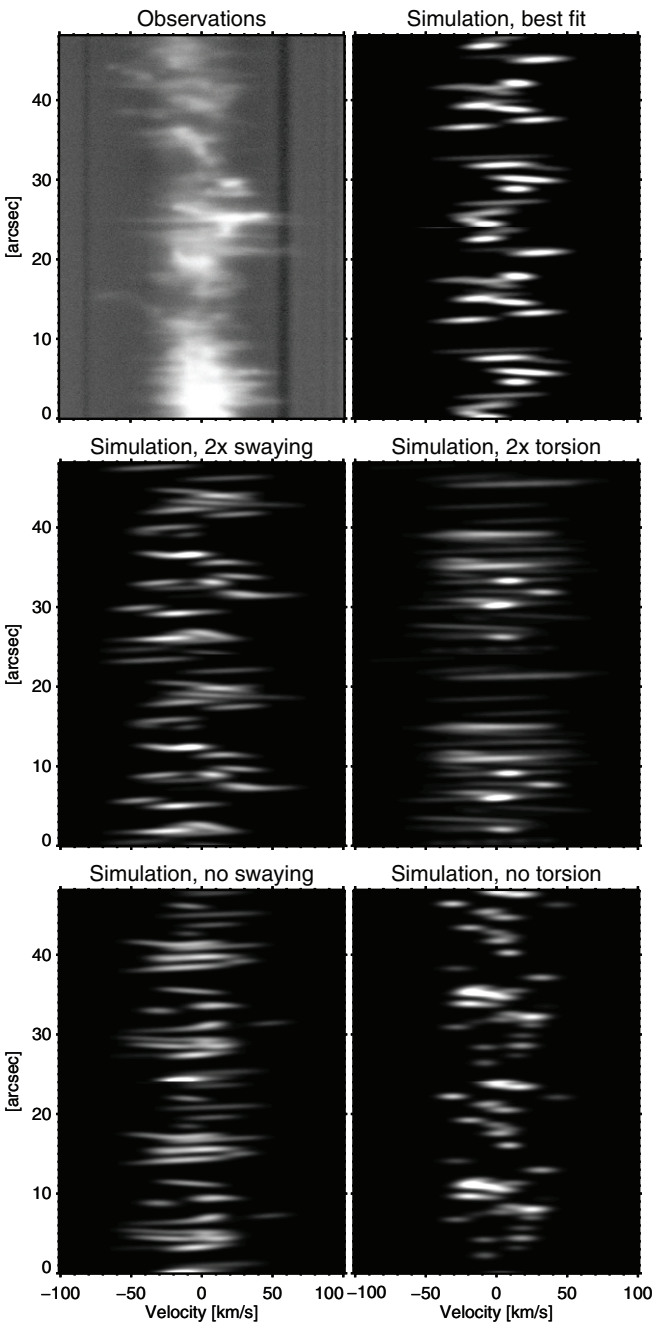

Figure 2. Comparison between observations and Monte Carlo simulations in $\lambda-y$ displays. The best-fit solution has field-aligned velocities of 60 km s^{-1}, torsional velocities of 30 km s^{-1}, and swaying motions of 15 km s^{-1} with periods of 100–300 s. Significant discrepancies occur for larger swaying, more torsion, no swaying, and no torsion.

Examples are given in the lower rows of Figures 2 and 3. In the first panel of the second row (Figure 2), the mean swaying amplitude is doubled and gives an overall zig-zag pattern with too many extremes. Similarly, doubling the mean torsional amplitude gives streaks that are too wide in velocity. Removing the swaying (bottom left panel) produces too little zig-zag motion in $\lambda - y$. No torsional motion gives streaks that are too narrow in velocity. Similarly, in the $\lambda - t$ panels of Figure 3 doubling the frequencies to periods of 50–100 s of the swaying or torsional motion leads to too many wiggles, whereas lower frequencies (periods 300–600 s) yield too few wiggles. Note that it is more difficult to determine the periods since these

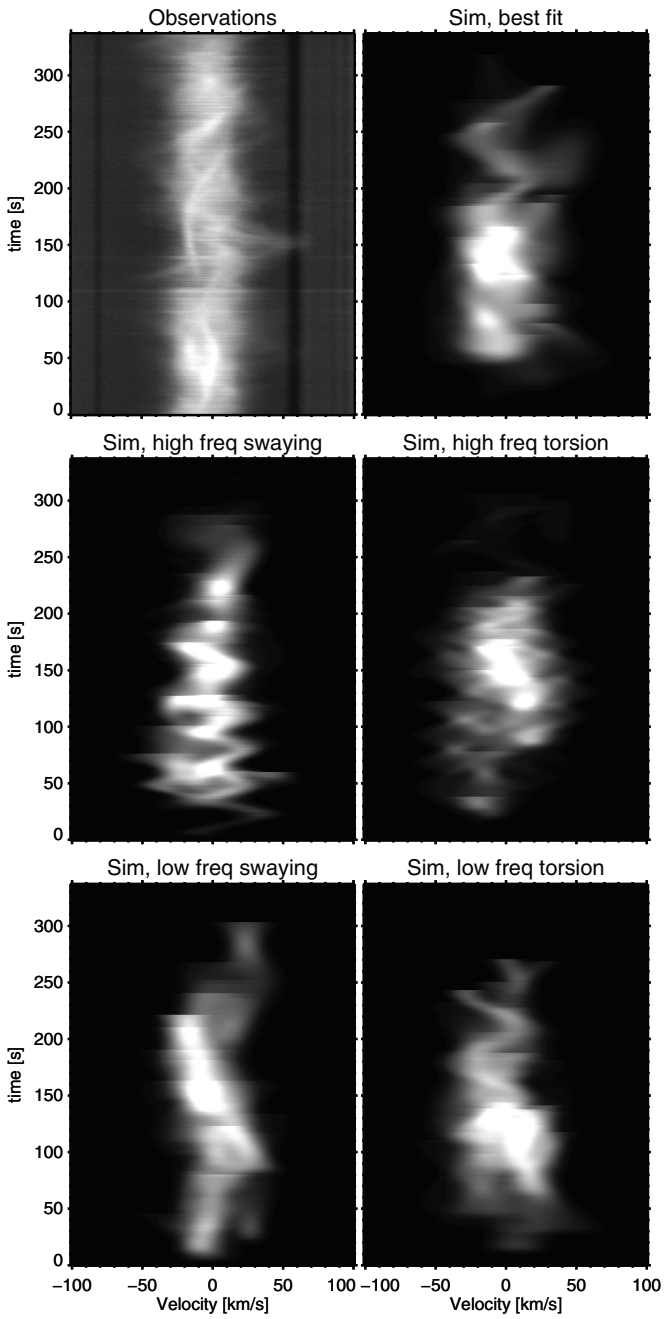

Figure 3. Comparison between observations and Monte Carlo simulations in $\lambda-t$ displays. The best-fit solution has field-aligned velocities of 60 km s^{-1}, torsional velocities of 30 km s^{-1}, and swaying motions of 15 km s^{-1} with periods of 100–300 s. Significant discrepancies occur for wave periods that are much higher or lower than these values.

often exceed the spicule lifetimes (see also De Pontieu et al. 2007c).

In summary, our Monte Carlo analysis provides reasonably well-defined constraints. In order to reproduce the appearance of our limb spectra the torsional and swaying motions should be of order 30 and 15 km s^{-1}, respectively, with periodicities of order 100–300s.

The next issue is whether the transverse swaying and torsional modulations represent propagating waves. Since our limb spectra sample only one height above the limb at a time, we address this question with CRISP imaging spectroscopy in Hα. The ultra-high cadence sequence permits the construction of Doppler images by subtracting the images taken in the red and blue wings (corresponding to $\pm$55 km s^{-1} Doppler shift). In these we often observe very fast propagation of the Doppler signal. An example is shown in Figure 4 where the apparent phase speed is 285 km s^{-1}. Values in the range 100–300 km s^{-1} are common. This is the order of magnitude expected for the Alfvén speed in structures with densities of order 10^{10} cm^{-3} (Beckers 1968) and magnetic field strengths of order 10–30 G (Centeno et al. 2010).

Determining whether these Doppler shift modulations represent swaying or torsional motion is not straightforward. In our Dopplergrams, torsional modulation will show up as a black-and-white pattern across a spicule only when the sum of the swaying motion and projection of the field-aligned flow happens to be zero. The large offsets from line center in Figure 1 suggest that such cancellation does not occur often. Direct separation of the torsional and swaying modes is impeded by the combination of very high phase speed, sparse wavelength sampling, and relatively low cadence, i.e., lack of simultaneity between the red- and blue-wing samplings. Nevertheless, the black-and-white pattern of the spicule at $t = 34.32$ s in Figure 4 seems to be direct evidence of significant torsional motion. Its propagation at about 300 km s^{-1} provides further support that the observed rotational motions are a signature of torsional Alfvén waves that propagate outward along spicules.

4. DISCUSSION

Our observations and analysis lead to the conclusion that spicules undergo three different types of motions at the same time: field-aligned flow aligned with the spicule axis, swaying that moves the spicule as a whole transverse to its axis, and torsional motion around its axis. The superposition of these motions complicates the interpretation of spicule spectroscopy and imaging considerably. Our Monte Carlo simulations served to disentangle them and indicate that our observations are compatible with field-aligned flows of order 50–100 km s^{-1}, swaying of order 15–20 km s^{-1}, and torsional motion of order 25–30 km s^{-1}. We also found evidence that the swaying and torsional motions are both signatures of Alfvénic waves with periods of order 100–300 s with propagation along the spicule axis at phase speeds as high as 100–300 km s^{-1}. Our data are inadequate to decide whether only upward propagation occurs, or whether propagation in both directions or even standing waves are as important for the torsional motions as they seem to be for swaying motions (Okamoto & De Pontieu 2011).

Our results impact several long-standing issues. First, any interpretation of observed spicular motion is likely wrong if not all three kinetic modes are properly accounted for. The classic reports of field-aligned outflows of order 20–30 km s^{-1} from Doppler shifts at the limb (e.g., Beckers 1972) did not include torsional and swaying contributions. This introduces additional uncertainty in the historically reported values for field-aligned spicular flows, which are already plagued by poor spatio-temporal resolution.

Second, juxtaposition of the three modes of motion explains the appearance of spicular features in the blue and red wings of Ca II 854.2 nm and Hα close to the limb. Such images show rows ("bushes") of near-vertical absorption features that are comparable to the on-disk "rapid blue excursions" (RBEs) of Rouppe van der Voort et al. (2009). When these are compared between near-simultaneous red and blue outer-wing samplings, the redshifted and blueshifted features appear with remarkably similar, though not identical, morphology and orientation.

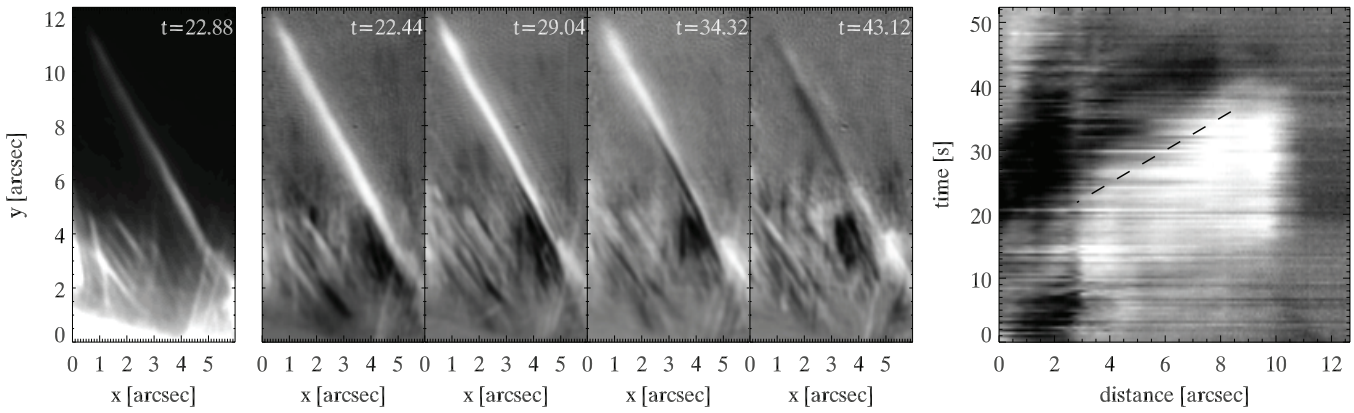

Figure 4. Example of sign change in spicule Doppler tilt in the ultra-high cadence (0.44 s) ±55 km s^{-1} CRISP Hα data. Left-hand panel shows an Hα wing image at maximum spicule length. Center panels contain sequences of four Doppler images at different sampling times (in seconds, blueshift bright). The right-hand panel shows space–time diagrams measured along the spicule axis. Dashed guidelines illustrate a propagation speed of 285 km s^{-1}.

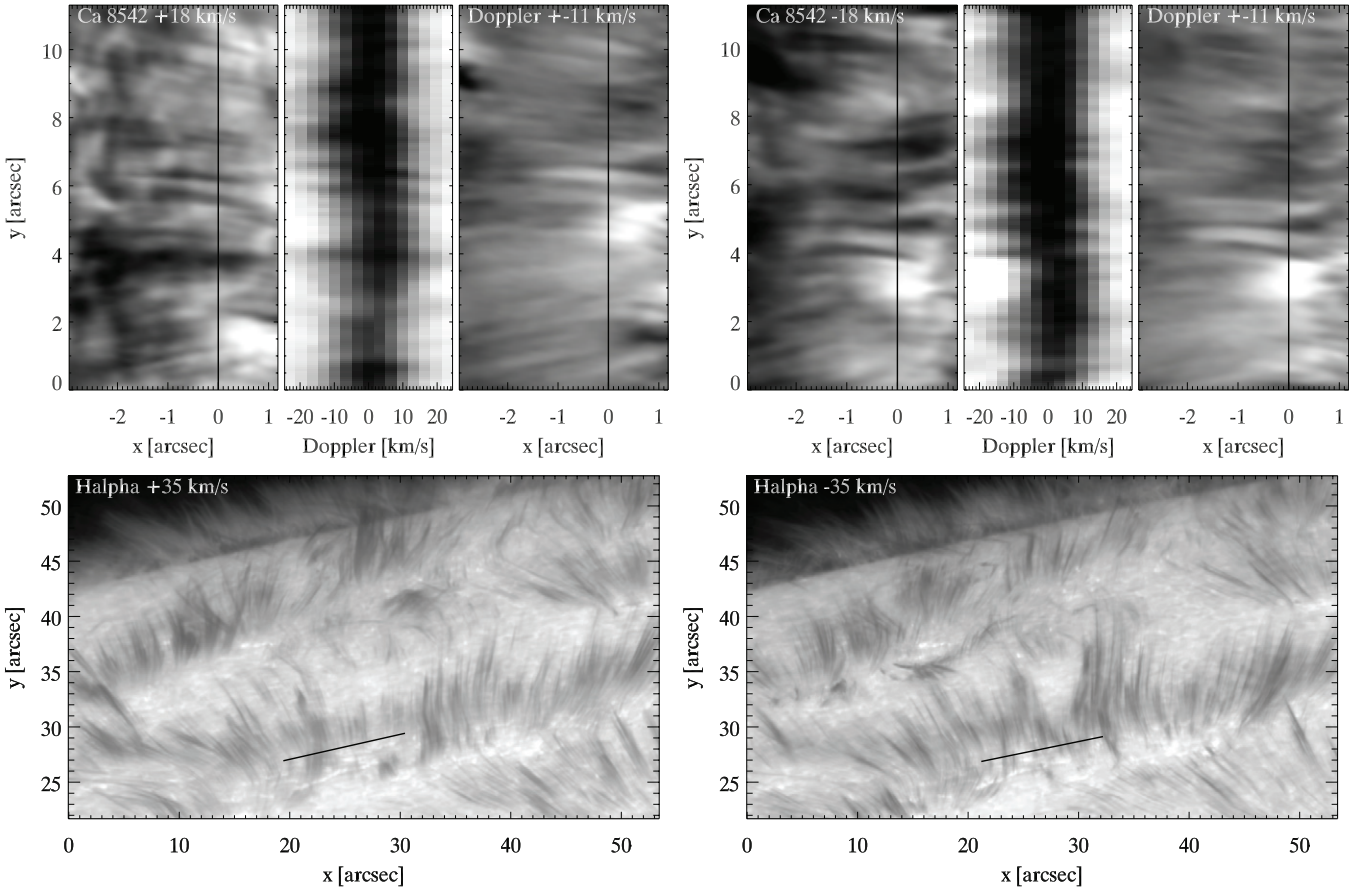

Figure 5. Two examples of CRISP Ca II 854.2 nm spectral behavior close to the limb, which is to the left (in top row). The slit-like sampling crossed a bush of near-limb spicules as shown by the black line in the Hα context images in the lower row. In the top row, each Ca II $\lambda - y$ diagram is accompanied by two Ca II slit-jaw images that have the location of the slit marked by a black line, at left a wing image, at right a Doppler image. The Ca II spectrograms and images were taken 17 s apart, the right-hand trio first. The Hα images were taken within a few seconds of each other 34 s later.

Precise fine-scale overlap is rare but the bush patterns often appear roughly the same. An Hα example pair is shown in the lower panels of Figure 5. Such outer-wing similarity has been interpreted as the presence of similar field-aligned flows pointing toward and away from the observer (Beckers 1972), but the asymmetry of near-limb line-of-sight projection should then cause large morphological inequality. It is much more likely that large-amplitude transverse motions dominate the visibility close to the limb of outer-wing features and that they cause morphological equality through near-cospatial and alternating red and blue Doppler shift modulations. The upper panels of Figure 5 indeed show spicular Doppler tilts in the central spectrum panels, much like the off-limb ones in Figure 1. This suggests that on-disk RBEs also undergo torsional motion.

Our observations confirm the speculation of Curdt & Tian (2011) that torsional motions likely occur on smaller scales than their SUMER observations of macrospicules and explosive events (or the so-called swirls; see Wedemeyer-Böhm & Rouppe

van der Voort 2009). Our results also support the early work by Avery (1970) and suggestions by Pasachoff et al. (1968) that upward propagating Alfvén waves explain indications of high-speed propagation of Doppler signals along spicules. The presence and/or observed periods of propagating torsional Alfvén waves can in principle provide information about the thermodynamic and magnetic properties of the guiding structures (e.g., Routh et al. 2010; Verth et al. 2010). Such idealized models are not yet a good representation of actual, highly dynamic spicules but may illustrate the potential diagnostic value of spicular wave observations.

The ubiquity of torsional spicule motion also provides support for scenarios of spicule formation in which nonlinear coupling of torsional Alfvén waves to other wave modes on expanding flux tubes leads to significant field-aligned flows that drive the plasma upward (Hollweg et al. 1982; Sterling & Hollweg 1984; De Pontieu & Haerendel 1998; Kudoh & Shibata 1999; Matsumoto & Shibata 2010). However, none of these models can explain both the large observed field-aligned flows and the rapid heating to at least transition-region temperatures. This suggests that while torsional motions may play a role in providing upward momentum in spicules, other components of spicule formation are still missing.

While our Monte Carlo simulation assumes the presence of only the $m = 0$ torsional mode, the observations also show evidence for more complex torsional modes with $m > 0$ (see example at $y = 34''$ in the top left panel of Figure 1). Our results thus may provide support for the recent hypothesis (van Ballegooijen et al. 2011; Asgari-Targhi & van Ballegooijen 2012) that complex torsional motions are generated in the interaction between convective motions and photospheric flux tubes (see, e.g., the ubiquitous vorticity reported in recent simulations by Moll et al. 2011), and that they may be responsible for heating of the chromosphere and corona.

The observed torsional motions imply that spicules, given their ubiquity, play a major role in the transport of helicity through the solar atmosphere. In addition, our results suggest that the energy flux carried by Alfvénic motions into the corona and heliosphere may be twice as large as the previous estimates that were based on swaying motions only (De Pontieu et al. 2007c; McIntosh et al. 2011).

The Swedish 1 m Solar Telescope is operated by the Institute for Solar Physics of the Royal Swedish Academy of Sciences in the Spanish Observatorio del Roque de los Muchachos of the Instituto de Astrofísica de Canarias. D. H. Sekse, T. Leifsen, and G. Vissers acquired the 2011 June 11 observations. This research was supported by the Research Council of Norway and by the European Union through the ERC Advanced Grant "Physics of the Solar Chromosphere." B. D. P. was supported through NASA grants NNX08BA99G, NNX08AH45G, and NNX11AN98G. The authors are grateful to Alan Title, Scott McIntosh, and Neil Murphy for insightful discussions.

REFERENCES

Asgari-Targhi, M., & van Ballegooijen, A. A. 2012, ApJ, 746, 81
Avery, L. W. 1970, Sol. Phys., 13, 301
Beckers, J. M. 1968, Sol. Phys., 3, 367
Beckers, J. M. 1972, ARA&A, 10, 73
Centeno, R., Trujillo Bueno, J., & Asensio Ramos, A. 2010, ApJ, 708, 1579
Curdt, W., & Tian, H. 2011, A&A, 532, L9
Curdt, W., Tian, H., & Kamio, S. 2012, Sol. Phys., in press
De Pontieu, B., & Haerendel, G. 1998, A&A, 338, 729
De Pontieu, B., Hansteen, V. H., Rouppe van der Voort, L., van Noort, M., & Carlsson, M. 2007a, ApJ, 655, 624
De Pontieu, B., McIntosh, S., Hansteen, V. H., et al. 2007b, PASJ, 59, 655
De Pontieu, B., McIntosh, S. W., Carlsson, M., et al. 2011, Science, 331, 55
De Pontieu, B., McIntosh, S. W., Carlsson, M., et al. 2007c, Science, 318, 1574
De Pontieu, B., McIntosh, S. W., Hansteen, V. H., & Schrijver, C. J. 2009, ApJ, 701, L1
Hansteen, V. H., De Pontieu, B., Rouppe van der Voort, L., van Noort, M., & Carlsson, M. 2006, ApJ, 647, L73
Hollweg, J. V., Jackson, S., & Galloway, D. 1982, Sol. Phys., 75, 35
Houtgast, J., & Namba, O. 1979, Proc. R. Neth. Acad. Arts Sci., 82, 223
Kiselman, D., Pereira, T. M. D., Gustafsson, B., et al. 2011, A&A, 535, A14
Kosugi, T., Matsuzaki, K., Sakao, T., et al. 2007, Sol. Phys., 243, 3
Kudoh, T., & Shibata, K. 1999, ApJ, 514, 493
Langangen, Ø., Carlsson, M., Rouppe van der Voort, L., & Stein, R. F. 2007, ApJ, 655, 615
Langangen, Ø., De Pontieu, B., Carlsson, M., et al. 2008, ApJ, 679, L167
Martínez-Sykora, J., Hansteen, V., & Moreno-Insertis, F. 2011, ApJ, 736, 9
Matsumoto, T., & Shibata, K. 2010, ApJ, 710, 1857
McIntosh, S. W., de Pontieu, B., Carlsson, M., et al. 2011, Nature, 475, 477
McIntosh, S. W., De Pontieu, B., & Tarbell, T. D. 2008, ApJ, 673, L219
Moll, R., Cameron, R. H., & Schüssler, M. 2011, A&A, 533, A126
Okamoto, T. J., & De Pontieu, B. 2011, ApJ, 736, L24
Pasachoff, J. M., Noyes, R. W., & Beckers, J. M. 1968, Sol. Phys., 5, 131
Rouppe van der Voort, L., Leenaarts, J., de Pontieu, B., Carlsson, M., & Vissers, G. 2009, ApJ, 705, 272
Rouppe van der Voort, L. H. M., De Pontieu, B., Hansteen, V. H., Carlsson, M., & van Noort, M. 2007, ApJ, 660, L169
Routh, S., Musielak, Z. E., & Hammer, R. 2010, ApJ, 709, 1297
Scharmer, G. B., Bjelksjo, K., Korhonen, T. K., Lindberg, B., & Petterson, B. 2003, Proc. SPIE, 4853, 341
Scharmer, G. B., Narayan, G., Hillberg, T., et al. 2008, ApJ, 689, L69
Sterling, A. C. 2000, Sol. Phys., 196, 79
Sterling, A. C., Harra, L. K., & Moore, R. L. 2010, ApJ, 722, 1644
Sterling, A. C., & Hollweg, J. V. 1984, ApJ, 285, 843
Suematsu, Y., Ichimoto, K., Katsukawa, Y., et al. 2008, in ASP Conf. Ser. 397, First Results From Hinode, ed. S. A. Matthews, J. M. Davis, & L. K. Harra (San Francisco, CA: ASP), 27
Suematsu, Y., Wang, H., & Zirin, H. 1995, ApJ, 450, 411
van Ballegooijen, A. A., Asgari-Targhi, M., Cranmer, S. R., & DeLuca, E. E. 2011, ApJ, 736, 3
van Noort, M., Rouppe van der Voort, L., & Löfdahl, M. G. 2005, Sol. Phys., 228, 191
Verth, G., Erdélyi, R., & Goossens, M. 2010, ApJ, 714, 1637
Wedemeyer-Böhm, S., & Rouppe van der Voort, L. 2009, A&A, 507, L9